INT. J. REMOTE SENSING, 1987, VOL. 8, NO. 7, 1093–1100

An explanation of enhanced radar backscattering from flooded forests

J. A. RICHARDS

Centre for Remote Sensing, University of New South Wales, Kensington, New South Wales 2033, Australia

P. W. WOODGATE

Department of Conservation, Forests and Lands, East Melbourne, Victoria 3002, Australia

and A. K. SKIDMORE

School of Forestry, Australian National University, Canberra, Australian Capital Territory 2600, Australia

(Received 27 November 1986; in final form 8 April 1987)

Abstract. A simple structural backscatter model for a forest stand, suitable for use with L-band HH polarized radar imagery, is used to explain the increased level of backscattering observed from flooded forests. Measurements made of relative levels of backscatter from SIR-B image data of a flooded Australian forest are consistent with an interpretation based upon scattering mechanisms involving both the tree components and the understorey or forest floor. The change in Fresnel power reflection coefficient of the ground with flooding is advanced as the cause of the enhancement in backscattered power levels.

1. Introduction

Studies with Seasat and aircraft imaging radar systems have demonstrated that the backscattering observed from forest stands may be enhanced under flood conditions (MacDonald *et al.* 1980, Ormsby *et al.* 1985, Ford *et al.* 1985). This implies that the backscattering mechanism involves energy that is returned to the radar via the forest floor or understorey, and indeed the effect has been attributed to forward scattering from the foliage to the forest floor, followed by specular or near-specular reflection back to the radar (Engheta and Elachi 1982). Recent modelling studies suggest, however, that for moderately sized trees (about 20 m high) and for moderately dense forest stands (typically 20 trees per 20 m × 20 m cell) the foliage-to-ground multiple reflection path is considerably weaker than multiple scattering from the trunk and ground, in which the trunk and ground together act in the manner of a dihedral corner reflector (Richards *et al.* 1987). This mechanism appears also to dominate over canopy volume scattering and sub-canopy surface scattering for typical forests, at least at L-band. Since it depends upon specular or near specular reflection from the floor, it also provides an explanation for the enhanced backscatter observed with flooded forests. It is the purpose of this paper to pursue this explanation in relation to an example of an Australian flooded forest observed in SIR-B image data.

2. The study site

SIR-B data take 115.8 were acquired on 13 October 1984 for a natural eucalypt forest situated on the Murray River, along the border between the states of New South

Wales and Victoria in Australia. Known as the Barmah–Millewa forest, it owes its continued well-being to regular flooding of the Murray. About 15 000 years ago a 10 m high fault line developed in a north–south direction across the course of the westward-flowing Murray, effectively damming the river and causing it to diverge into two arms, one to north and the other to the south. The large triangular sedimentary basin that formed is now subject to periodic flooding caused by high winter and spring precipation in the headwaters of the Murray. The forest, which dominates the flood plain, consists of virtually pure monospecific stands of River Bed Gum (*Eucalyptus camaldulensis*) owing to this species' unique adaption to regular flooding. In lower-lying areas of the delta, shallow lakes and swamps are in various stages of siltation. Aeolin sand hills rise up to 12 m above the flood plain and support Yellow Box (*Eucalyptus melliodora*) and Grey Box (*Eucalyptus microcarpa*). Local variation in topography is however generally less than 2 m.

Comprehensive forest type and site quality maps exist for the Barmah–Millewa forest, having been prepared by the Forestry Commission of New South Wales and the Victorian Department of Conservation, Forests and Lands. The value of SIR-B imagery as a supplement to Landsat multispectral scanner data for mapping the forest into these units has been considered by Skidmore *et al.* (1986). That exercise was complicated however by the presence of a flood at the time of SIR-B data acquisition, owing to the major influence of standing water on the forest backscatter characteristics.

3. Radar imagery and flood records

Figure 1 shows SIR-B radar data of the forest region under consideration, along with Landsat multispectral scanner visible and infrared imagery of the area. The latter was acquired on 17 November 1984, from which the forest outline can be readily determined. Inspection of the radar image reveals the essential shape of the forest in the

(*a*)

(*b*)

(*c*)

Figure 1. (*a*) SIR-B image and Landsat MSS (*b*) visible and (*c*) infrared image data of the Barmah–Millewa forest recorded respectively in October and November 1984. Note the protrusion of the forest to the south in the Landsat data that is not as bright in the backscatter image.

enhanced backscattering tone; however, there are some discrepancies, the most notable of which being a protruding portion of the forest to the south that is not as bright. The brighter regions correspond to a major flood within the forest, while the darker regions of the forest have a dry understorey. The flood was classed by the forest authorities as being of 80 per cent magnitude, in that 80 per cent of the forest floor was estimated to be inundated.

Maps of 80 per cent floods from 1969 and 1984 were available to the project: generally a better correspondence however was found between the 1969 map and the radar flood boundaries than with the 1984 map. This is not surprising owing to the limited sampling used to obtain the 1984 maps and the consequent latitude for error. Remarks in the following therefore relate to the flood boundaries mapped in 1969. Details from the 1969 map were digitized by the authors onto the radar imagery in order to associate known flooding regimes with the radar backscattering observations. This is shown in figure 2. As can be seen, there is generally good agreement of map features with corresponding aspects in the radar data. The only significant difference lies in the nature of the ponding that occurs in the southernmost unflooded segment of forest.

4. Explanation of enhanced backscatter

Richards *et al.* (1987) have suggested that four components should be included in developing a backscatter model for forests at L-band. These are depicted in figure 3 and include volume scattering from the canopy, diffuse scattering from the forest floor, scattering from the canopy to the floor followed by specular reflection to the radar, and a similar mechanism involving the trunk. Combining these to develop a composite backscattering coefficient generates dependences upon incidence angle, average tree height and average stand density that agree well with SIR-B image data recorded over northern California conifer forests. Even though tree structures in the Barmah–Millewa region are quite different, the essential principles of the model are the same and can be used as guidelines in explaining backscatter measurements.

Of the two scattering paths in figure 3 that involve reflection from the ground, Richards *et al.* noted that the trunk–ground term is about 20 dB higher than the foliage–ground term at incidence angles around 40° for HH polarization with trees 20 m high and with stand densities of 20 trees per 20 m × 20 m radar resolution cell. The average tree height and density in the Barmah–Millewa forests are in excess of these values; in consequence the trunk–ground term would be expected to be higher still than the volume forward scattering mechanism. Moreover in the mid range incidence angles the trunk–ground term for those tree and stand characteristics is larger than any of the other contributions by at least 10 dB, allowing that term to be considered alone in interpreting tree backscattering data at L-band for HH polarization. It is only when trunk heights are as small as 10 m that the trunk-ground term reduces to a magnitude comparable to the other mechanisms.

Interpreted as an equivalent dihedral corner reflector, the radar cross section of a single tree can be expressed (Richards *et al.* 1986) as

$$\sigma_{t,s} = \sigma_{dcr} R_t R_g \exp(-2kh_c \sec\theta)\Gamma(\theta,\lambda)$$

in which σ_{dcr} is the cross-section of an ideal corner reflector of the same dimensions as the tree, h_c is the equivalent thickness of the tree canopy and k is the attenuation coefficient of the canopy. $\Gamma(\theta,\lambda)$ is a correction factor used to match $\sigma_{t,s}$ to the

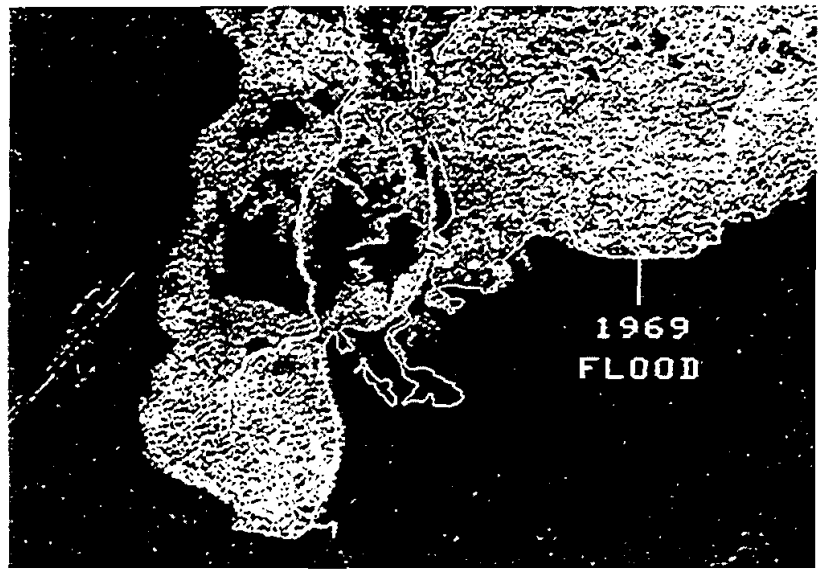

(*a*)

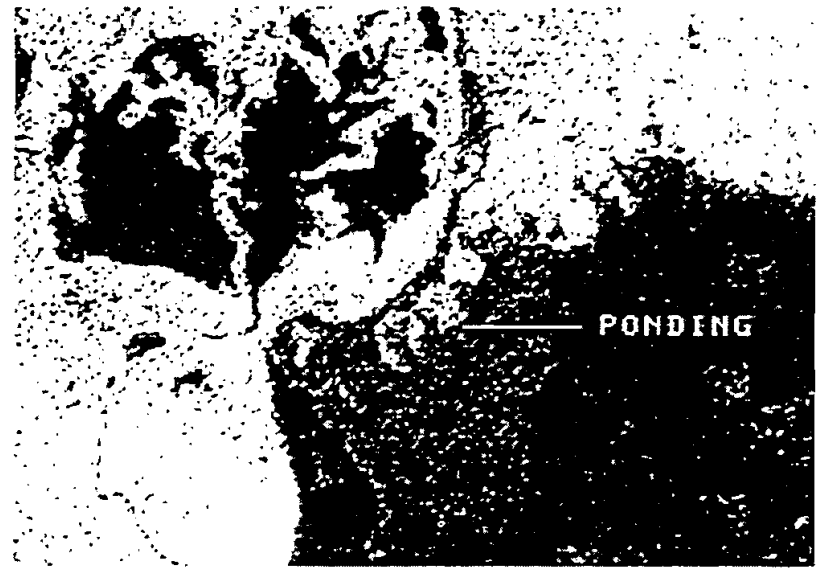

(*b*)

Figure 2. (*a*) Mapped flood boundaries from 1969 superimposed over the radar image illustrating the association of enhanced backscatter with flooding regimes. (*b*) Expanded portion clearly showing the ponding formed under the forest.

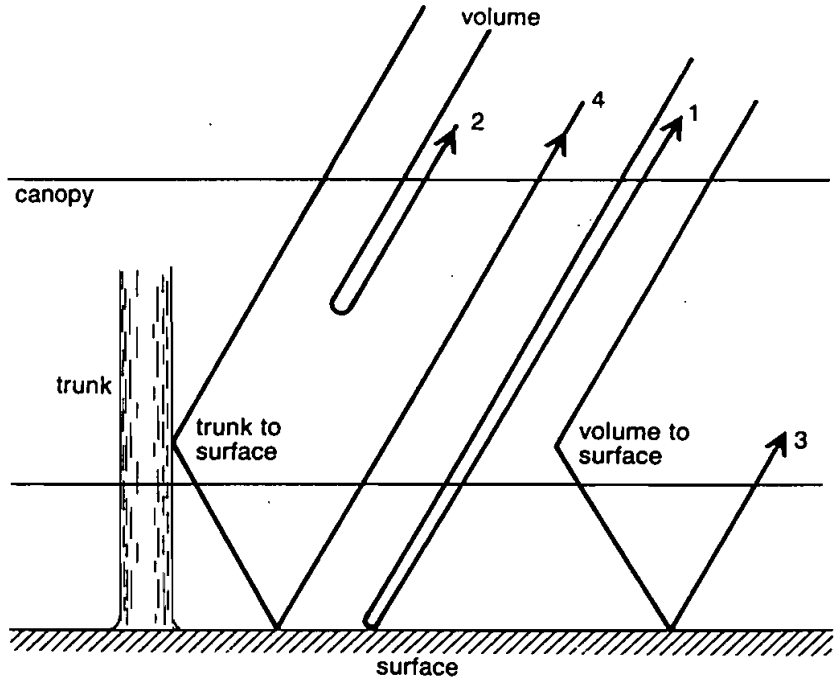

Figure 3. Four essential components of backscatter from a forest stand (after Richards *et al.* 1987).

backscattering coefficient for a dielectric cylinder over a plane over the range of tree diameters considered significant; θ is the incidence angle. R_t and R_g are the Fresnel power reflection coefficients at the air–trunk and air–ground interfaces respectively. It is via the latter that the effect of changes in the forest floor composition enters backscatter calculations. For an air–ground boundary R_g is given by

$$R_g = |\rho_g|^2$$

where

$$\rho_g = \frac{\cos\theta - \sqrt{(\varepsilon - \sin^2\theta)}}{\cos\theta + \sqrt{(\varepsilon - \sin^2\theta)}}$$

for HH polarization, in which ε is the dielectric constant of the ground.

Figure 4 shows values of $\sigma_{t,s}$ as a function of ε over a range from that corresponding to dry sandy soil (~ 2) to that for water (~ 80), normalized to the case for a ground Fresnel reflection coefficient of unity. Three curves are shown corresponding to incidence angles of 20° (Seasat SAR) and 36·3° (SIR-B data take 115.8), and with 60° as an extreme value. This demonstrates that if flooding occurs over a dry sandy forest floor the observed backscatter coefficient will increase by about 8 dB; the increase for flooding of a loamy forest floor will be about 5 dB for data take 115.8.

To assess the increased backscatter resulting from flooding in the forested SIR-B image of figure 2, five areas of flooded forest and five in the dry region were selected from which mean SIR-B image brightnesses were computed. The means were squared to allow relative backscatter to be computed. This showed an enhanced backscattering of the flooded region over forest with a dry understorey of 6·75 dB, consistent with a

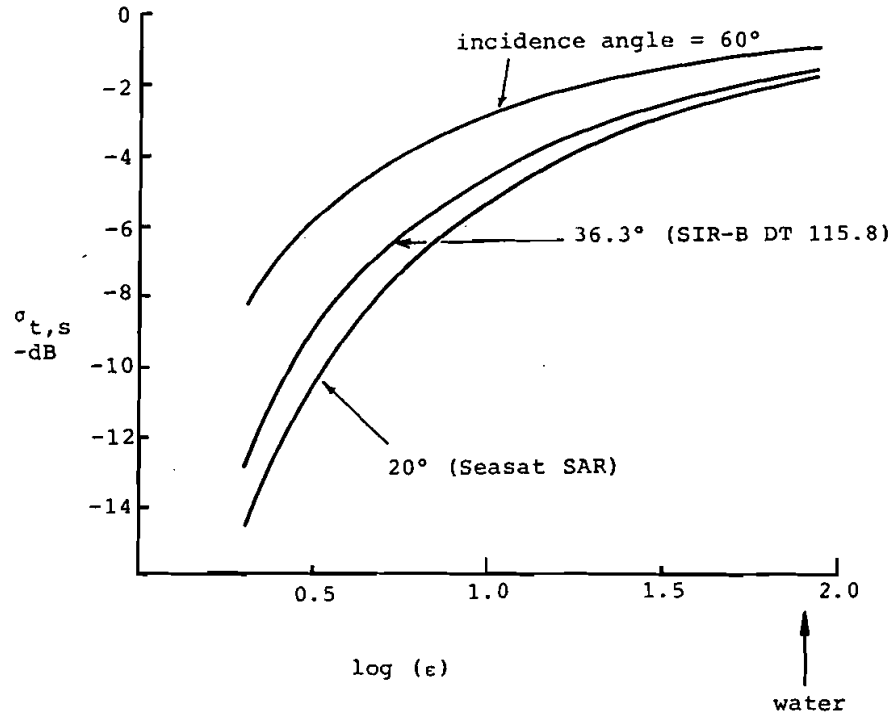

Figure 4. Normalized radar cross-section for the trunk–ground combination as a function of the ground dielectric constant over the range $\varepsilon = 2$ to 80. Values of cross-section are normalized to that corresponding to a Fresnel power reflection coefficient of the ground of unity.

dry loam forest floor before flooding. A better estimate of the difference in backscatter demands that the noise level in the image be determined and this subtracted from the measurements before a comparison is made. For this purpose, the mean brightness of three lakes was determined and used to correct the flooded and dry understorey forest backscattering values. The backscatter enhancement then becomes 10·8 dB which seems implausibly high if attributed simply to a change from soil to water, as a specular surface under the forest canopy. However if the ground under the forest is considered a diffuse reflector when dry, it is possible that 10 dB of enhancement may occur with flooding. For example a Lambertian soil surface would give 1·9 dB less forward reflection than one which behaves specularly, leading to an overall enhancement in backscattering of about 9·7 dB for a loam forest basement when flooded.

5. Concluding remarks

Figure 4 shows that enhancements of up to 12 dB or so are possible in principle after flooding from forest floors that are originally dry sand, and that larger enhancements would be expected with smaller angles of incidence. Whether this explains fully the increased backscatter noted in the Barmah–Millewa forest SIR-B image, or whether there is a need to consider also more precise presentation of the scattering properties of the dry surface, is not of major significance. Rather, the general principle of the explanation has been demonstrated and reinforces the notion that

forest backscatter is dominated by a component that undergoes reflection from the forest floor. Should this have been a weak component, such as forward scattering from the canopy, the enhancement noted with standing water would have been weaker.

It is important to emphasize that the dominance of the trunk-ground scattering mechanism has only been demonstrated for L-band HH radar. At C-band, and especially X-band, when canopy attenuation and volume scattering will be higher than at L-band, the same differential of backscatter would not be expected with flooding since less energy will penetrate the canopy on both the forward and reflected paths.

The strength of the backscatter relative to a dry understorey makes L-band radar a convenient tool by which to map forest flooding with a high degree of detail. The expanded section shown in figure 2(*b*) demonstrates the identification of ponding under the forest and shows clearly the streams from the main flood that feed the ponds.

Acknowledgments

The authors are grateful to the Victorian Department of Conservation, Forests and Lands for providing flood boundary maps. This work was supported by the Australian Research Grants Scheme.

References

ENGHETA, N., and ELACHI, C., 1982, Radar scattering from a diffuse vegetation layer over a smooth surface. *I.E.E.E. Transactions on Geoscience and Remote Sensing*, **20**, 212–216.

FORD, J. P., WICKLAND, D. E., and SHARITZ, R. R., 1985, Mapping diverse forest cover with multi-polarization aircraft radar. In *NASA/JPL Aircraft SAR Workshop Proceedings*, edited by N. Donovan, D. Evans and D. Held (JPL Publication 85–39), pp. 53–56.

MACDONALD, H. C., WAITE, W. P., and DEMARCKE, J. S., 1980, Use of Seasat satellite radar imagery for the detection of standing water beneath forest vegetation. *American Society of Photogrammetry Annual Technical Meeting*, Niagara Falls, New York.

ORMSBY, J. P., BLANCHARD, B. J., and BLANCHARD, A. J., 1985, Detection of lowland flooding using active microwave systems. *Photogrammetric Engineering and Remote Sensing*, **51**, 317–328.

RICHARDS, J. A., SUN, G.-Q., and SIMONETT, D. S., 1987, L-band radar backscatter modeling of forest stands. *I.E.E.E. Transactions on Geoscience and Remote Sensing*, **25**, No. 4.

SKIDMORE, A. K., WOODGATE, P. W., and RICHARDS, J. A., 1986, Classification of the Riverina Forests of south eastern Australia using co-registered Landsat MSS and SIR-B radar data. *Proceedings of the Symposium Commission VII International Society for Photogrammetry and Remote Sensing*, Enschede, September, pp. 517–519.